Balancing accuracy, efficiency, and flexibility in radiation calculations for dynamical models

Robert Pincus[1,2], Eli J. Mlawer[3], Jennifer S. Delamere[4]

[1]Cooperative Institute for Environmental Studies, University of Colorado, Boulder, Colorado, USA

[2]NOAA/Earth System Research Lab, Physical Sciences Division, Boulder, Colorado, USA

[3]Atmospheric and Environmental Research, Lexington, Massachusetts, USA

[4]Alpenglow Scientific, Fairbanks, Alaska, USA

Key Points:

- RTE+RRTMGP is a new freely-available toolbox for radiation calculations for dynamical models
- RTE+RRTMGP seeks to balance accuracy, efficiency, and flexibility, defined expansively
- Both code and data continue to evolve to explore different balances among these goals

Corresponding author: Robert Pincus, `Robert.Pincus@colorado.edu`

Abstract

This paper describes the initial implementation of new toolbox that seeks to balance accuracy, efficiency, and flexibility in radiation calculations for dynamical models. The toolbox consists of two related code bases: Radiative Transfer for Energetics (RTE) computes fluxes given a fully-specified radiative transfer problem, and RRTM for GCM applications - Parallel (RRTMGP), which maps a physical description of the gaseous atmosphere into a radiative transfer problem. The toolbox is an implementation of well-established ideas, including the use of a k-distribution to represent the spectral variation of absorption by gases and the use of two-stream, plane-parallel methods for solving the radiative transfer equation. The focus is instead on accuracy, by basing the k-distribution on state-of-the-art spectroscopy, and on the sometimes-conflicting goals of flexibility and efficiency. Flexibility is facilitated by making extensive use of computational objects encompassing code and data, the latter provisioned at run time and potentially tailored to specific problems. The computational objects provide robust access to a set of high-efficiency computational kernels that can be adapted to new computational environments. Accuracy is obtained by careful choice of algorithms and through tuning and validation of the k-distribution against benchmark calculations.

1 Why build another radiation parameterization?

The ultimate energy source for all atmospheric motions is electromagnetic radiation emitted by the sun and by the planet and its atmosphere. The flow of radiative energy through the atmosphere depends strongly on the state of the surface and the atmosphere itself. Essentially any model of the atmospheric motions, therefore, has to represent the flow of radiation through the atmosphere, especially the vertical gradients within the atmosphere that give rise to heating and cooling, and the fluxes of radiation absorbed at the surface. Models aimed at understanding climate must also accurately compute the net energy at the top of the atmosphere.

The representation of radiation is one of the most pure exercises in parameterization in atmospheric models because the solution to fully-specified problems is known to great accuracy. (This can be contrasted with convection parameterizations, for example, for which sensitive dependence on initial conditions make fully deterministic prediction essentially impossible, or cloud microphysics, for which some governing equations are not known.) Accuracy across a wide range of clear-sky conditions can be measured

by comparison to benchmark models (Oreopoulos et al., 2012; Pincus et al., 2015) which are themselves known to be in excellent agreement with observations (Mlawer et al., 2000; Turner et al., 2004; Alvarado et al., 2013). Benchmark models also exist for clouds though observational validation is far more challenging.

The ideas underlying state-of-the-art radiative transfer parameterizations have been established for decades. Radiation is assumed not to propagate in the horizontal (the Independent Column Approximation), reducing the dimensionality of the radiative transfer problem. The complex spectral structure of absorption by gases is treated by grouping optically-similar spectral regions using either a correlated k-distribution (e.g. Lacis & Oinas, 1991; Fu & Liou, 1992) or, less commonly, by modeling transmission using an exponential sum fit of transmissivities (Wiscombe & Evans, 1977). The optical properties of condensed materials, such as clouds and aerosols, are computed in advance, usually as functions of one or more bulk parameters such as effective radius, and fit to tables or functional forms. The resulting problem is solved using versions of the radiative transfer equation in which the angular dependence has been reduced analytically. Though innovations continue, for example in efforts to treat the impact of three-dimensional transport on radiation fields (Schäfer et al., 2016; Hogan et al., 2016), major conceptual advances in the parameterization of radiation are infrequent.

The maturity of ideas, the near-universal need for radiation parameterizations, and the substantial effort involved in building an end-to-end parameterization mean that radiation codes tend to be developed as complete packages, and that these packages, and especially the interfaces to them, have long lifetimes. The codes used by the UK Met Office have their roots in the work of Edwards & Slingo (1996). In the United States many atmospheric models, including both regional and global models developed at the National Center for Atmospheric Research and the National Weather Service's Global Forecast System, use RRTMG (Mlawer et al., 1997). These packages are comprehensive, using information about the physical state of the atmosphere to provide values of spectrally-integrated radiative flux.

But conceptual maturity and the black-box nature of radiation codes can hide important errors. The accuracy of radiation parameterizations can be judged by comparison to reference line-by-line models with high angular resolution; every such comparison over the last two-and-a-half decades (e.g. Ellingson et al., 1991; Collins, 2001; Ore-

opoulos et al., 2012; Pincus et al., 2015) has identified significant parameterization errors in the treatment of gaseous absorption and scattering. These errors partly reflect different efforts to balance computational cost and accuracy, but they also arise because groups may be slow to incorporate new spectroscopic knowledge. Updates to the widely-used HITRAN database (Rothman et al., 2009, 2013) over the last decades, for example, have tended to increase the amount of solar radiation absorbed by water vapor. Underestimating this absorption has important consequences for calculations of hydrologic sensitivity (Fildier & Collins, 2015; DeAngelis et al., 2015). The likelihood of errors increases when parameterizations are used to make calculations far outside the range of conditions on which they are trained, for example in calculations on exoplanets (e.g. Yang et al., 2016). Even the highly-elevated concentrations of CO_2 frequently used to estimate climate sensitivity (Gregory, 2004) represent a challenge for some parameterizations (Pincus et al., 2015).

Complete packages developed for one application may not be easy to adapt to unforeseen uses. Every existing radiation package of which we are aware assumes a particular orientation in the vertical dimension, requiring the reordering of data when the convention in the radiation package differs from that of the host model. Many require separate clear- and all-sky calculations at each invocation where only the latter are needed to advance the host model. None that we're aware of provide the ability to specify an upper boundary condition, so that their use in models with shallow domains requires the specification of an atmospheric profile for use in the radiation scheme alone, complicating implementation and requiring unnecessary computation. In practice, too, most packages tightly couple two conceptually-different problems: the mapping of atmospheric state to optical properties, and the subsequent calculation of fluxes (i.e. determining the radiative transfer problem and determining the solution to a given problem). This tight coupling makes it difficult to explore algorithms in which access to the underlying spectral structure is required (e.g Pincus & Stevens, 2009, 2013).

Finally, while every process parameterization seeks to minimize computational cost, efficiency is an acute concern for radiation packages because each calculation is so time-consuming that radiation is typically computed less frequently than other processes by factors of 10-20 (see, for example, section 2.1 in Hogan & Bozzo, 2018). Computational efficiency is not a static target, however, because computing platforms changes rapidly even if the underlying algorithms do not. Even today an implementation that is efficient

on traditional processors is likely to be poorly structured for specialized but highly-efficient hardware such as general-purpose Graphical Processing Units (GPUs).

This paper describes the initial implementation of new toolbox that seeks to balance accuracy, efficiency, and flexibility in radiation calculations for dynamical models. The toolbox consists of two related code bases: Radiative Transfer for Energetics (RTE) computes fluxes given a fully-specified radiative transfer problem, and RRTM for GCM applications - Parallel (RRTMGP), which maps a physical description of the aerosol- and cloud-free atmosphere into a radiative transfer problem. Although every line of RTE+RRTMGP is new, the code descends from RRTMG (Mlawer et al., 1997; Iacono et al., 2000; Clough et al., 2005), a parameterization with similar capabilities developed roughly 20 years ago. It also incorporates many of the lessons learned in the development of PSrad (Pincus & Stevens, 2013), a re-implementation of RRTMG built to explore an idea that required extensive refactoring of the original code. Like its predecessors RRTMGP uses a k-distribution for computing the optical properties and source functions of the gaseous atmosphere based on profiles of temperature, pressure, and gas concentrations, while RTE computes fluxes using the Independent Column Approximation in plane-parallel geometry.

Below we describe how the design of RTE+RRTMGP balances the sometimes-conflicting goals of accuracy, efficiency and flexibility, explain how the k-distributions are constructed, and assess the accuracy of the current model against more detailed calculations.

2 An extensible architecture for flexibility

The calculation of radiative fluxes for dynamical models presents a particular computational challenge among parameterizations. To treat the enormous spectral variability of absorption by the many optically-active gases in the atmosphere, a relatively small amount of state information, i.e. profiles of temperature, pressure, and gas concentrations, must be mapped into optical properties (the parameters need to solve the radiative transfer equation) at a number of spectral quadrature points. Fluxes are computed independently at each spectral quadrature point. Users, however, are normally interested only in integrals over the spectrum (or portions of it), so spectrally-resolved fluxes are summed, greatly reducing the amount of data used by the host model.

As a result of this structure the radiation problem has an exceptional opportunity to exploit fine-grained parallelism. Much of the problem is atomic, meaning that calcu-

lations are independent in space and the spectral dimension. Transport calculations are independent in the spectral and horizontal dimensions (the latter as a result of the Independent Column Approximation), while spectral reduction is independent in both the horizontal and vertical dimensions. Exploiting this parallelism is key to computational efficiency although the optimal ordering varies across different stages of the computation. RTE and RRTMGP operate on multiple columns at a time to exploit this parallelism. The column dimension is inner-most; despite good reasons for having the spectral dimension vary fastest (Hogan & Bozzo, 2018) this choice allows user control over vector length and can be easily adapted to different architectures.

RTE and RRTMGP are agnostic to the ordering of the vertical axis.

2.1 Designing for robustness

Like the recently-developed ecRad package (Hogan & Bozzo, 2018) RTE+RRTMGP cleanly separates conceptually-distinct aspects of the radiation problem from one another. Each component, including the gas optics and source function calculations, any implementations of aerosol and cloud optics, and methods for computing radiative transfer (transport), can be modified or replaced independently. RTE+RRTMGP is implemented in Fortran 2003. Many components are implemented as Fortran classes that package together code and data. As described below many of the classes are user-extensible to permit greater flexibility. The radiative transfer solvers are straightforward functions.

The Fortran 2003 classes simplify control and information passing, as described below, but basic computational tasks are isolated as kernels, simple procedures with language-neutral interfaces. The computational kernels are implemented in Fortran 90 with C-language bindings including the explicit run-time specification of array sizes. Kernels expect sanitized input and do no error checking, so they can be quite compact and efficient. Separating computational kernels from flow control is also intended to enhance flexibility: it would be possible to build front ends in other languages including Python or C++, using the Fortran class structure or any alternative that suited the problem at hand, and still exploit the efficient Fortran kernels. It would also be possible to replace the default kernels with other implementations. We have explored this possibility in developing prototype kernels optimized for GPUs using OpenACC directives.

173 The class structure is also aimed at minimizing the amount of data passed to and

174 from the radiation calculation, reducing latency and increasing efficiency when radiation

175 is implemented on dedicated computational resources (e.g. Balaji et al., 2016) and es-

176 pecially on devices such as GPUs.

177 Other conventions aim to make RTE+RRTMGP more portable across platforms

178 and environments. The precision of all REAL variables is explicitly set via a Fortran KIND

179 parameter so that a one character change in a single file can produce single- or double-

180 precision versions of the code. RTE+RRTMGP uses few thresholds but most are expressed

181 relative to working precision. Most procedures are implemented as functions returning

182 character strings; empty strings indicate success while non-empty strings contain error

183 messages. RTE+RRTMGP does not read or write to files: classes which require data such

184 as lookup tables at initialization use load functions with flat array arguments so that users

185 can read and distribute data consistent with their local software environment.

2.2 Specifying and solving the radiative transfer equation: RTE

186

187 The components of RTE+RRTMGP communicate through sets of spectrally-dependent

188 optical properties. Optical properties are described by their spectral discretization: the

189 number of bands and the spectral limits of each band in units of wavenumber (inverse

190 centimeters). Each band covers a continuous region of the spectrum but bands need not

191 be disjoint or contiguous. Anticipating the spectral structure provided by gas optics pa-

192 rameterizations like RRTMGP, each band may be further sub-divided into g-points. Each

193 spectral point is treated as a independent pseudo-monchromatic calculation.

194 Optical properties may be specified as sets of numerical values on a column/height/spectral

195 grid. Optical properties might be only the absorption optical depth τ_a, as is required for

196 computing radiative transfer in the absence of scattering; the set of extinction optical

197 depth τ_e, single-scattering albedo ω_0, and asymmetry parameter g used in two-stream

198 calculations; and the set of τ_e, ω_0, and phase function moments p required by four-stream

199 or other discrete ordinates calculations. (The dependence on two spatial coordinates and

200 a spectral coordinate is left implicit.)

201 Each possible set of values is represented as a discrete sub-class of the general op-

202 tical properties class. Using a class structure allows user interaction to be greatly sim-

203 plified. As one example, sets of optical properties on the same grid can be added together

204 in a single call, with the class structure invoking the correct kernel depending on which

205 two sets of optical properties are provided. Single calls allow optical properties to be delta-

206 scaled (Potter, 1970; Joseph et al., 1976) or checked for erroneous values.

207   Solvers compute radiative fluxes given values of optical properties and appropri-

208 ate boundary conditions and source function values. A shortwave solver requires spec-

209 ifying the (pseudo-)spectrally-dependent collimated beam at the top of the model and

210 albedos for direct and diffuse radiation at the surface in addition to the values of opti-

211 cal properties within the atmosphere. A longwave solver requires the surface emissiv-

212 ity and the values of the Planck source functions from the surface and at each layer and

213 level of the atmosphere.

214   Calculations that account for scattering, the usual standard for shortwave radia-

215 tion and a more accurate option for longwave calculations that include clouds (Costa &

216 Shine, 2006; Kuo et al., 2017), use the two-stream formulation of Meador & Weaver (1980)

217 to compute layer transmittance and reflectance and the adding formulation of Shonk &

218 Hogan (2008) to compute transport (i.e. the fluxes that result from interactions among

219 layers). Two-stream coupling coefficients in the shortwave come from the "practical im-

220 proved flux method" formulations of Zdunkowski et al. (1980); the longwave follows Fu

221 et al. (1997). The accuracy of longwave calculations that neglect scattering may be in-

222 creased through the use of first-order Gaussian quadrature using up to three terms us-

223 ing weights and directions of Clough et al. (1992). Longwave calculations assume that

224 the source function varies linearly with optical depth. At this writing RTE does not yet

225 include four-stream or higher-order methods for radiative transport.

226   The set of optical properties provided determines the solution method: when the

227 solvers are called with the sub-class representing $\{\tau, \omega_0, g\}$ the two-stream/adding solver

228 is invoked; if only τ is provided, a calculation neglecting scattering is performed. Solu-

229 tions are computed for each g-point in the set of optical properties independently, allow-

230 ing RTE to solve problems for any spectral structure.

231   All solvers allow for the specification of incoming diffuse radiation at the top of the

232 domain (this flux is otherwise assumed to be 0). We originally imagined that this capa-

233 bility would be most useful in the simulation of very shallow domain by fine-scale mod-

234 els (e.g. Seifert et al., 2015). Experience implementing RTE+RRTMGP in global mod-

els, however, suggests that it may also be a useful alternative to the common practice of adding an extra layer above the model top in radiation calculations.

Because radiative fluxes are computed from optical properties there is no explicit treatment of clouds, and particularly of internal cloud variability or its structure in the vertical. Subgrid variability may be accounted for by random sampling in the spectral dimension using the Monte Carlo Independent Column Approximation (Pincus et al., 2003) but treatments that rely on an explicit clear/cloudy partitioning, including the Triple-Clouds algorithm for treating partial cloudiness (Shonk & Hogan, 2008) or the SPAR-TACUS extension for treating the subgrid-scale effects of three-dimensional radiative transport (Schäfer et al., 2016; Hogan et al., 2016), are not consistent with this framework.

The RTE solvers compute fluxes for each spectral point independently but the full spatial and spectral detail is unlikely to be useful in most contexts. It is, on the other hand, hard to know precisely what users might need. One approach would be to implement an expansive set of output variables, perhaps allowing user control over which are computed, but this can be cumbersome and requires changes to the radiation code to add a new output.

RTE takes a conceptually more complicated but practically simpler approach: output from RTE solvers is provided through a user-extensible Fortran 2003 class. The class must include storage for the desired results and code to compute or reduce those results from the full profiles of fluxes at each spectral point. In particular the class must implement a reduction function (so-named because it reduces the amount of output) with arguments specified by RTE. These arguments include the spectral discretization information and the vertical ordering, enabling the computation of very specific quantities (during design we had in mind the calculation of photosynthetically-active radiation at the surface). Examples are provided that compute broadband fluxes (spectrally-integrated up, down, net, and direct if available) and fluxes within each band. Users provide this class in the call to the solver; the solvers, in turn, call the reduction function after spectrally-dependent fluxes are calculated, minimizing the amount of information returned from RTE.

2.3 Computing the optical properties of the gaseous atmosphere: RRT-MGP

RTE provides methods for solving a spectrally-detailed radiative transfer problem; its complement, RRTMGP, determines the parameters of such a radiative transfer problem for the gaseous component of the atmosphere given the physical state and composition. RRTMGP encapsulates the calculation of gas optics, i.e. the calculation of τ_a or $\{\tau_e, \omega_0, g\}$ and the associated source functions given pressure, temperature and gas concentrations within the domain. RRTMGP builds on RTE: the classes representing gas optics and the Planck functions extend the generic representation of optical properties, and the gas optics calculation returns a set of optical property values.

RRTMGP includes a general framework for representing gas optics. One piece of this framework is a class describing the concentrations of gases within the atmosphere. The volume mixing ratio of each gas is provided as a name-value pair, where the name is normally the chemical formula (e.g. 'ch4' or 'h2o'). Values may be provided as scalars, if the gas is well-mixed; as profiles assumed constant in the horizontal; or varying in the horizontal and vertical dimensions.

The second piece of the general framework, an abstract gas optics class, defines a minimal set of interfaces for functions that map atmospheric state to optical properties. Codes written to use this generic interface can seamlessly use any concrete instance of the abstract class. This approach is motivated by the desire to explore hierarchies of detail in the treatment of absorption by gases (Vallis et al., 2018; Tan et al., 2019) without requiring substantial re-coding.

RRTMGP gas optics is a concrete instance of the abstract gas optics class that uses a k-distribution to represent the spectral variation of absorption coefficients. Data and code are entirely distinct in RRTMGP's gas optics: the class is initialized with data provided in a netCDF file (though RRTMGP does not read the file directly, for reasons explained above). The ability to provide data at run time, available for more than 20 years in the radiation codes used by the UK Met Office (Edwards & Slingo, 1996), provides flexibility, including the provisioning of data with accuracy matched to application needs, as well as a way to incorporate new spectroscopic knowledge as it become available, so that models can stay up-to-date without code changes. The class representing gas concentrations must also be supled when initializing RRTMGP gas optics, so that the ta-

bles of absorption coefficients may be thinned to include only those gases for which concentrations are provided, reducing impacts on memory and computation time.

2.4 Mapping concepts to software

Figure 1 illustrates the class structure by which RTE+RRTMGP is organized. The figure highlights the capabilities described in Sections 2.2 and 2.3. Not shown are initialization and finalization procedures, procedures for extracting subsets from values defined with a column dimension (available for source functions, optical properties, and gas concentrations), or the procedures by which the spectral discretization can be set and queried.

Figure 1 emphasizes the distinction between optics, which map atmospheric conditions defined on a spatial grid onto spectrally-dependent values of optical properties and source functions, and stored sets of these values defined on a spatial and spectral grid. RRTMGP is a map for the gaseous component of the atmosphere. As we note above, users must provide analogous maps for condensed species. In most applications users will initialize these maps (e.g. RRTMGP gas optics, user-provided aerosol and cloud optics) with data at the beginning of a simulation. Each calculation of radiative fluxes made during the course of a simulation uses those maps to determine the optical properties of each component of the atmosphere, defines a set of problems to be solved (e.g. clear-sky as the sum of gases and aerosols and all-sky as the sum of clear-sky and clouds), and invokes the solvers on each problem, summarizing results to meet (problem-specific) user requirements.

3 Accuracy and efficiency

3.1 Developing a new treatment of absorption by gases

RRTMGP treats absorption by gases using a k-distribution (Ambartsumian, 1936; Goody et al., 1989; Lacis & Oinas, 1991; Fu & Liou, 1992) in which an integral over frequency ν is replaced by an integral over the variable g defined such that absorption coefficient $k(g)$ increases monotonically (and hence much more smoothly); this integral is further approximated by a discrete sum over G quadrature points using an average absorption coefficient at each point. The mapping $\mathcal{M}_{\nu \to g}$ is normally computed for a set of bands within which absorption is dominated by one or two gases though alternatives

are possible (Hogan, 2010). The map varies with the state of the atmosphere, so there is no inherent mapping between g-points and wavelengths. For RRTMGP the bands are disjoint, contiguous, and essentially span the set of frequencies of radiation emitted by the sun or earth.

As is described in more detail below, the k-distribution is first generated for a range of atmospheric conditions following an automated procedure, then tuned by adjusting these absorption coefficients (and the related "Planck fractions" described below) by hand so that fluxes and their sensitivity to composition perturbations, computed over a set of training profiles, are in agreement with line-by-line reference calculations. The Appendix contains greater detail about the k-distribution and and how it is discretized.

3.1.1 *Automated generation of a k-distribution*

The version of RRTMGP data described here is based on high-accuracy calculations with the Line-By-Line Radiative Transfer Model (LBLRTM; Clough et al., 2005), which has undergone extensive cycles of evaluation with observations and subsequent improvement (see, e.g., Mlawer et al., 2012; Alvarado et al., 2013) and agrees with well-calibrated spectrally resolved radiometric measurements. Results below are based on LBLRTM_v12.8, line parameter file aer_v_3.6 (itself based to a large extent on the HITRAN 2012 line file described by Rothman et al. (2013)), and continuum model MT_CKD_3.2. All are available from `https://rtweb.aer.com`. Shortwave calculations are based on the solar source function of Lean & DeLand (2012).

In the automated step, computations of optical depth are made with LBLRTM for a set of pressure and temperature values spanning the range of present-day conditions to define the spectral map. Reference volume mixing ratios $\hat{\chi}_i$ for water vapor and ozone are based on a large number of profiles from the MERRA-2 reanalysis (Randles et al., 2017) and vary with temperature, with distinct reference values for pressures greater than or less than 10000 Pa. Other species use a constant reference value.

RRTMGP follows RRTMG in defining bands so that absorption within each band is dominated by no more than two gases termed that band's "major species." Some bands have no major species. Dry air is used as the second major species in bands in which absorption is dominated by a single gas, which allows the use of a single method in all bands to account for the dependence of the k-distribution on the varying abundances of ma-

jor species. Computations are made for range of relative abundances $0 \leq \eta \leq 1$ of the two major species where $\eta \equiv \tilde{\chi}_1/(\tilde{\chi}_1 + \tilde{\chi}_2)$ and $\tilde{\chi}_i$ denotes volume mixing ratio χ_i normalized by its reference value $\hat{\chi}_i(p, T)$, with concentrations of all other gases held fixed at their respective reference values. The total optical depth, including contributions from major and all minor species, determines the spectral map $\mathcal{M}_{\nu \rightarrow g}(p, T, \eta)$.

Given this spectral map, the absorption coefficients for the major species are derived from LBLRTM calculations of absorption optical depth $\tau_a(p, T, \eta)$ in single atmospheric layers containing only the major species in question. Optical depth values are mapped from frequency ν to g, averaged across a pre-determined number G of g intervals, and converted to absorption coefficients $k(g)$ by dividing by the combined column amount $W = W_1 + W_2 \times \hat{\chi}_1/\hat{\chi}_2$, where W_i is defined as the layer-integrated molecular amount (molecules cm^{-2}) of major species i.

For longwave bands the same mapping $\mathcal{M}_{\nu \rightarrow g}(p, T, \eta)$ is used to calculate the "Planck fraction," defined as the fraction of the band-integrated Planck energy (uniquely determined by T) associated with each g-point within the band. The solar source function for each g-point is constant at present; the Appendix describes how these values are obtained.

The contributions of other absorbing species are handled with less detail than are major species. A single representative pressure $p_0(T)$ is chosen for each "minor species." LBLRTM is used to calculate the spectrally-dependent absorption coefficient of this species in isolation as a function of temperature. The coefficients are ordered using $\mathcal{M}_{\nu \rightarrow g}(p_0(T), T, \eta)$ and averaged within each of the G intervals. Rayleigh scattering optical depths follow the same approach.

Absorption by both major and minor species is treated separately in the upper and lower atmosphere (pressures above and below 10000 Pa). Distinct sets of gases are used in each domain. Some gases are considered below 100 hPa but not above, or vice versa, depending on the degree to which they influence fluxes.

The discretization of the k-distribution available at this writing, including details about the spectral discretization ("bands"), the gases considered within each band, and the density of the tabulated data, are provided in the Appendix. Given this tabulated information, RRTMGP computes absorption coefficients and Planck fractions for arbi-

388 trary atmospheric conditions by linearly interpolating the tabulated values in $\ln(p)$, T,

389 and η. Optical depths are computed by multiplying the interpolated absorption coeffi-

390 cient by the combined column amount of the layer in question. Interpolation algorithms

391 are as general as possible so that, for example, the same code is used for contributions

392 that depend only on absorber abundance and those that also depend on the abundance

393 of other gases, such as collision-induced absorption and foreign continua. Planck source

394 functions are determined by multiplying these Planck-fractions by band-integrated Planck

395 source functions tabulated on a fine temperature grid.

3.1.2 Testing and tuning the correlated k-distribution

397 We evaluate the accuracy of the initial k-distribution by computing fluxes for a set

398 of 42 clear-sky atmospheric profiles (Garand et al., 2001) that span a large range of tem-

399 perature, moisture, and ozone abundances, and include baseline concentrations of other

400 gases. Results from RTE+RRTMGP for these training atmospheres are compared to LBLRTM

401 calculations. We minimize differences due to transport algorithms by using the same set

402 of quadrature angles in LBLRTM and RTE for longwave problems; in the shortwave we

403 focus on the direct beam since this depends only on the optical depth. For shortwave

404 assessments the solar zenith angle is 30 degrees; for longwave calculations the surface emis-

405 sivity is 1.

406 Fluxes computed across the set of atmospheres using the initial k-distribution are

407 in substantially better agreement with reference calculations than are fluxes computed

408 with RRMTG (Figure 2), primarily because RRTMGP is based on the same underly-

409 ing spectroscopy as the benchmark.

410 We also assess the accuracy of RRTMGP in computing instantaneous radiative forc-

411 ing, i.e. the change in flux for these 42 profiles due to increases, relative to nominal pre-

412 industrial concentrations, of factors of two and four for CO_2 and CH_4 and the change

413 between present-day and pre-industrial concentrations of N_2O and halocarbons. The pri-

414 mary focus is on $4\times CO_2$ and $2\times CH_4$.

415 Accuracy assessments for both flux and forcing guide a hand-tuning of the absorp-

416 tion coefficients and source functions. This tuning is holistic, considering a wide range

417 of radiative quantities but focusing primarily on broadband flux and heating rate pro-

418   files and the forcing due to individual gases, especially CO_2 and CH_4. Attention is also

419   paid to flux and heating rate profiles within each band to minimize compensating errors.

420   In calculations with RTE, the optical properties and source functions provided by

421   RRTMGP gas optics at each g-point are treated as a set of pseudo-monochromatic cal-

422   culations. This is equivalent to assuming that the spectral mapping (or "correlation" be-

423   tween ν and g) is constant through the atmosphere, and is what distinguishes a corre-

424   lated k-distributions used in vertically inhomogeneous atmosphere from a k-distribution

425   developed for a single layer. The assumption is an important source of error in corre-

426   lated k-distributions. In many circumstances the true spectral map varies in the verti-

427   cal, such that the absorption coefficients for a g-value correspond to different sets of fre-

428   quencies at different altitudes. As one example, in shortwave bands in which ozone and

429   water vapor both absorb significantly, absorption in the stratosphere is dominated by

430   ozone with a very different spectral structure than the absorption by water vapor in the

431   troposphere, yet absorption due to these two gases will map to the same g-values at dif-

432   ferent altitudes. In such circumstances the lack of consistency with height of the spec-

433   tral map $\mathcal{M}_{\nu \to g}(p, T, \eta)$ (a lack of correlation) degrades model accuracy relative to spectrally-

434   resolved calculations.

435   The hand-tuning attempts to correct for these and any other errors. Major species

436   coefficients are adjusted as functions of p and η; minor species coefficients are tuned as

437   functions of T. The ad hoc and empirical tuning is similar in sprit to, but substantially

438   less formal than, the work reported by Sekiguchi & Nakajima (2008), who used an ex-

439   plicit cost function to determine the spectral discretization and integration rules for their

440   k-distribution.

441   Tuning modestly improves the accuracy of the k-distribution (compare orange and

442   green boxes in Fig. 2), decreasing both the bulk of errors and the most extreme errors

443   in our training atmospheres. Forcing is also improved (see the examples in Figure 3). In

444   interpreting these results recall that the profiles used here are chosen to explore specific

445   sources of error rather than being strictly representative of the distribution of conditions

446   in the Earth's atmosphere.

3.2 Accuracy: validation and verification

Before comparing results from RTE+RRTMGP against reference calculations we verified RTE against ecRad (Hogan & Bozzo, 2018) by computing broadband fluxes for the training atmospheres with both codes using RRTMGP's representation of gas optics. Differences in fluxes are within 10^{-8} W/m^2 for direct and diffuse shortwave fluxes, reflecting the fact that both packages make the same choices even though they are entirely independent implementations. Differences in longwave fluxes are as large as 10^{-2} W/m^2 due to different formulations of the source function.

The accuracy of fluxes at the atmosphere's boundaries computed by RTE+RRTMGP in its most commonly-used configuration is shown in Figure 4; RRTMG is show for comparison. Here longwave fluxes are computed with a single angle and total fluxes (diffuse plus direct for the shortwave) computed for the training atmospheres are compared against reference line-by-line calculations using three angles. Calculations with RRTMG use a diffusivity angle that depends on column-integrated water vapor in some bands to mimic the three-angle calculation (e.g. Fig. 2). The lack of this correction in RRTMGP increases the error in downwelling longwave flux at the surface in some atmospheres. (We are currently developing a similar treatment of diffusivity angle for RRTMGP.) Changes in other fluxes are dominated by revisions to spectroscopy, so that RRTMGP is substantially more accurate then RRTMG.

Figure 5 shows the maximum magnitude of heating rate errors. Pressures greater and less than 10000 Pa are shown separately because radiative heating rates are much larger in the latter than the former.

We assess the out-of-sample accuracy of RTE+RRTMGP using 100 profiles chosen by the Radiative Forcing Model Intercomparison Project (RFMIP) protocol (Pincus et al., 2016). The profiles were drawn from reanalysis so that the weighted sum of fluxes in the profiles reproduces the change in global-mean, annual-mean top-of-atmosphere present-day to pre-industrial forcing (the change in flux between atmospheres with present-day and pre-industrial concentrations of greenhouse gases). Relative to high angular-resolution line-by-line calculations with LBLRTM, fluxes computed by RTE+RRTMGP are accurate to within 0.4% at the top of the atmosphere and 0.2% at the surface; absorption by the atmosphere is accurate to about 0.4% for the longwave and 0.8% for the shortwave (see Table 1). Pre-industrial to present-day changes at the atmospheres boundaries

Table 1. Error (and reference value) of annual-mean, global-mean instantaneous radiative forcing (W/m^2), for present-day relative to pre-industrial conditions, computed using 100 profiles following the protocol of the Radiative Forcing Model Intercomparison Project. Error is computed relative to reference calculations with high angular and spectral resolution. The columns are chosen to characterize the error in forcing; as one consequence average values for fluxes in the present-day (the first set of columns) is affected by sampling error.

	Present-day fluxes		Pre-industrial to present-day change	
	Longwave	Shortwave	Longwave	Shortwave
Top of atmosphere (up)	0.033 (263.197)	0.165 (47.315)	0.148 (-2.845)	0.007 (-0.058)
Net absorption	-0.749 (-180.696)	-0.610 (72.344)	-0.055 (0.803)	-0.051 (0.522)
Surface (down)	0.725 (315.346)	0.026 (245.553)	-0.095 (2.083)	0.065 (-0.534)

are accurate to roughly 5% for longwave change and 12% for the (substantially smaller) shortwave change.

3.3 Efficiency

As one measure of efficiency we compare the time taken to compute clear-sky flux profiles for the 1800 atmospheric conditions (100 profiles for each of 18 perturbations to atmospheric conditions) used in the RFMIP assessment of accuracy. On a dedicated compute node at the National Energy Research Scientific Computing Center, using current Intel compilers and processing 8 columns at a time, RRTMGP is slower than RRTMG by roughly a factor of 2.2 in longwave calculations. RRTMG uses substantially fewer spectral points (140 in the longwave) than does RRTMGP (256); even accounting for this difference RRTMGP remains about 20% slower than its predecessor. The inefficiency is mostly due to the calculations of gas optics and Planck sources. It arises partly because RRTMGP takes a general approach to the calculation of gas optical depths, where RRTMG's compute paths (e.g. which gases contributed to absorption in each band) were coded by hand and so were more easily optimized. We are working to refactor a few closely-related routines to further increase the computational efficiency. In the shortwave, on the other hand, RRTMGP is about as twice as fast as RRTMG, or almost 4 times faster per g-point, owing primarily to easily-vectorized codes. We have noted substantial variation

in these ratios across computing platforms, operating systems, and compilers, and caution that real-life applications may be less efficient than these idealized tests.

4 Tools and packages

This paper stresses the principles guiding the development and use of RTE+RRTMGP. This is partly because we expect the underlying software to evolve and partly because the principles – designing parameterizations for flexibility and efficiency from the ground up – may be useful in designing other parameterizations. We have stressed our intent to make RTE+RRTMG as flexible as possible with respect to both the computing environment and the context in which radiative calculations are to be made.

One consequence of agnosticism with respect to the host model is that users have substantially more responsibility. This is most obvious in the treatment of clouds and aerosol. The RTE+RRTMGP repository includes examples to compute cloud optics (the map from physical state to optical properties), using a class analogous to the RRTMGP gas optics, and to treat cloud overlap with the Monte Carlo Independent Column Approximation (Pincus et al., 2003), using procedures relying on user-generated random numbers. The examples are narrow by design and are directly useful only if the assumptions about macro- and micro-physics are consistent with the host model's. The intent of the examples is to be useful as a starting point from which users may build implementations more self-consistent with the host model's other formulations. The programs used to compute accuracy for RFMIP in section 3.2, also included in the RTE+RRTMGP repository, show how the RRTMGP gas optics is initialized from data and used to compute the inputs needed for RTE, and how output is extracted from RTE, and play a similar role.

Many of the concerns that spurred the development of RTE+RRTMGP have motivated other development efforts. One example is the ecRad code (Hogan & Bozzo, 2018), which was developed contemporaneously. Compared to RTE+RRTMGP, ecRad is more complete (it includes treatments for cloud and aerosol optics and carefully-crafted methods for sub-grid scale sampling of homogenous clouds) and more capable (it includes alternatives for treating cloud overlap and a parameterization for three-dimensional transport within each column). The ecRad package represents a complete solution suitable for users who want to make precisely the same choices or are willing to adapt the inter-

nals of the package to their own needs. RTE+RRTMGP, in contrast, is intended as an extensible tool or platform on which user-specific applications can be built by extension rather than modification.

Optics computations - the mapping from model state to a radiative transfer problem - are a form of coupling in which detailed information about both representations is required. From this perspective the role of RTE is to provide a reasonably flexible representation of the radiative transfer problem and a matched set of methods for solution. The coupling of clouds and aerosols to these problems is left to users because the variety of possible macro- and micro-physical descriptions is enormous while the tools required to make the map, such as codes for computing single-scattering properties using Mie-Lorenz theory, are widely accessible. Computing the optical properties of the gaseous atmosphere, on the other hand, requires a small and easily enumerable set of inputs but relies on tools and expertise that is less broadly distributed among the community. These considerations explain our choice to link RTE+RRTMGP in both the software sense and in this description.

This paper reports on the initial implementation of RTE+RRTMGP. In particular the assessments of accuracy in Section 3 use a k-distribution with 16 g-points per band, for a total of 256 in the longwave and 224 in the shortwave. Experience developing the predecessor RRTMG from its parent model suggests that much of the accuracy of the underlying k-distribution can be obtained with substantially fewer spectral points (see also Sekiguchi & Nakajima, 2008), making possible substantial increases in efficiency for modest decreases in accuracy. We also anticipate that accuracy in clearly defined applications such as weather forecasting may be able to achieve the same accuracy with less computational cost by reducing the number of spectral points that provide accuracy in instantaneous radiative forcing. We are currently working to provide several sets of absorption coefficients striking different balances between accuracy and efficiency.

A   RRTMGP's *k*-distribution in detail

Tables A.1 and A.2 show the band structure adopted in the present version of RRTMGP. The band values in the longwave differ modestly from those in RRTMG. The ordering of shortwave bands is strictly montonic, abandoning the idiosyncratic ordering of RRTMG. Both changes imply that any fits e.g. for cloud optical properties made for RRTMG will need to be revisited before use in RRTMGP.

The spectral map $\mathcal{M}_{\nu \to g}(p, T, \eta)$ is computed at pressures $1 \leq p \leq 109600$ Pa in increments of $\ln(p) = 0.2$, temperatures $160 \leq T \leq 355$ K in 15 K increments, and $\eta = 0, 1/8, \ldots 1$. When computing η the mixing ratio of the second major gas v_2 is set to the reference value $\hat{v}_2(p, T)$ and v_1 varies except at $\eta = 1$, where $v_2 = 0$ and $v_1 = \hat{v}_1(p, T)$.

Band-integrated values of the Planck function are computed in 1 K increments.

589 The g-point dependence of the solar source function S is determined from the ref-
590 erence line-by-line calculations for the 42 atmospheres used for validation (Sec. 3.1.2).
591 For each profile i within this set and within each band b we identify the pressure $\check{p}_{i,b}$ at
592 which the direct solar beam has been depleted by 10% and compute the map at the cor-
593 responding values of T and η. Although the Garand et al. (2001) atmospheres span a
594 wide range of temperatures and gas abundances we find relatively little variation among
595 the maps $\mathcal{M}_{\nu \to g}^{i,b}(\check{p}_b, T^i(\check{p}_{i,b}), \eta(\check{p}_{i,b}))$. We therefore compute the average map across the
596 set of profiles and apply this map to the incident solar radiation to determine $S(g)$ for
597 all profiles.

References

599 Alvarado, M. J., Payne, V. H., Mlawer, E. J., Uymin, G., Shephard, M. W., Cady-
600   Pereira, K. E., ... Moncet, J. L. (2013). Performance of the Line-By-Line Ra-
601   diative Transfer Model (LBLRTM) for temperature, water vapor, and trace gas
602   retrievals: recent updates evaluated with IASI case studies. *Atmos. Chem. Phys.*,
603   *13*(14), 6687–6711.

604 Ambartsumian, V. (1936). The effect of absorption lines on the radiative equillib-
605   rium of the outer layers of stars. *Publ. Astron. Obser. Lenningrad*, *6*, 7–18.

606 Balaji, V., Benson, R., Wyman, B., & Held, I. (2016, October). Coarse-grained com-
607   ponent concurrency in Earth system modeling: parallelizing atmospheric radiative
608   transfer in the GFDL AM3 model using the Flexible Modeling System coupling
609   framework. *Geosci. Model Dev.*, *9*(10), 3605–3616.

610 Clough, S. A., Iacono, M. J., & Moncet, J.-L. (1992). Line-by-line calculations of at-
611   mospheric fluxes and cooling rates: Application to water vapor. *J. Geophys. Res.*,
612   *97*(D14), 15761–15785.

613 Clough, S. A., Shephard, M. W., Mlawer, E. J., Delamere, J. S., Iacono, M. J.,
614   Cady-Pereira, K., ... Brown, P. D. (2005, March). Atmospheric radiative transfer
615   modeling: a summary of the AER codes. *J. Quant. Spectrosc. Radiat. Transfer*,
616   *91*(2), 233–244.

617 Collins, W. D. (2001, November). Parameterization of Generalized Cloud Overlap
618   for Radiative Calculations in General Circulation Models. *J. Atmos. Sci.*, *58*(21),
619   3224–3242.

620 Costa, S. M. S., & Shine, K. P. (2006, April). An estimate of the global impact

Table A.1. Current RRTMGP spectral structure for the longwave. The distinction between major and minor absorbers is explained in Section 3.1. Water vapor foreign and self-continua are also included as minor gases for any bands in which water vapor is a major species.

Band	Wavenumber limits (cm^{-1})	absorbers ($p \geq 10000$Pa) major	minor	absorbers ($p < 10000$Pa) major	minor
1	10 - 250	H_2O	N_2	H_2O	N_2
2	250 - 500	H_2O		H_2O	
3	500 - 630	H_2O, CO_2	N_2O	H_2O, CO_2	N_2O
4	630 - 700	H_2O, CO_2		O_3, CO_2	
5	700 - 820	H_2O, CO_2	O_3, CCL_4, CFC-22	O_3, CO_2	CCL_4, CFC-22
6	820 - 980	H_2O	CO_2, CFC-11, CFC-12, HFC-143 a	—	CFC-11, CFC-12, HFC-143 a
7	980 - 1080	H_2O, O_3	CO_2	O_3	CO_2
8	1080 - 1180	H_2O	CO_2, O_3, N_2O, CFC-12, CFC-22, HFC-23 HFC-32, HFC-125, HFC-134 a	O_3	CO_2, CO, CFC-12, CFC-22, HFC-23, HFC-32, HFC-125, HFC-134 a
9	1180 - 1390	H_2O, CH_4	N_2O, CF_4, HFC-134 a, HFC-143 a	CH_4	N_2O, CF_4, HFC-134 a, HFC-143 a
10	1390 - 1480	H_2O		H_2O	
11	1480 - 1800	H_2O	O_2	H_2O	O_2
12	1800 - 2080	H_2O, CO_2		—	
13	2080 - 2250	H_2O, N_2O	CO_2, CO	—	O_3
14	2250 - 2390	CO_2		CO_2	
15	2390 - 2680	H_2O, CO_2	N_2O, N_2	—	
16	2680 - 3250	H_2O, CH_4		CH_4	

Table A.2. Current RRTMGP spectral structure for the shortwave. The distinction between major and minor absorbers is explained in Section 3.1. Water vapor foreign and self-continua are also included as minor gases for any bands in which water vapor is a major species.

Band	Wavenumber limits (cm^{-1})	absorbers $(p \geq 10000Pa)$ major	minor	absorbers $(p < 10000Pa)$ major	minor
1	820 - 2680	H_2O, CO_2	CH_4, N_2O, N_2	H_2O, CO_2	CH_4, N_2O, O_3
2	2680 - 3250	H_2O, CH_4		CH_4	
3	3250 - 4000	H_2O, CO_2		H_2O, CO_2	
4	4000 - 4650	H_2O, CH_4		CH_4	
5	4650 - 5150	H_2O, CO_2		CO_2	
6	5150 - 6150	H_2O	CH_4	H_2O	CH_4
7	6150 - 7700	H_2O	CO_2	H_2O, CO_2	
8	7700 - 8050	H_2O, O_2		H_2O, O_2	
9	8050 - 12850	H_2O	O_2	H_2O	O_3
10	12850 - 16000	H_2O, O_2	O_3	H_2O, O_2	O_3
11	16000 - 22650	H_2O	O_3, O_2, NO_2	O_3	O_2, NO_2
12	22650 - 29000	—	NO_2	—	NO_2
13	29000 - 38000	O_3		O_3	
14	38000 - 50000	O_3, O_2		O_3, O_2	

of multiple scattering by clouds on outgoing long-wave radiation. *Quart. J. Royal Met. Soc.*, *132*(616), 885–895.

DeAngelis, A. M., Qu, X., Zelinka, M. D., & Hall, A. (2015, December). An observational radiative constraint on hydrologic cycle intensification. *Nature*, *528*(7581), 249–253.

Edwards, J. M., & Slingo, A. (1996, April). Studies with a flexible new radiation code. I: Choosing a configuration for a large-scale model. *Quart. J. Royal Met. Soc.*, *122*(531), 689–719.

Ellingson, R. G., Ellis, J., & Fels, S. (1991). The intercomparison of radiation codes used in climate models: Long wave results. *J. Geophys. Res.*, *96*(D5), 8929–8953.

Fildier, B., & Collins, W. D. (2015, October). Origins of climate model discrepancies in atmospheric shortwave absorption and global precipitation changes. *Geophys. Res. Lett.*, *42*(20), 8749–8757.

Fu, Q., & Liou, K. N. (1992). On the correlated k-distribution method for radiative transfer in nonhomogeneous atmospheres. *J. Atmos. Sci.*, *49*(22), 2139–2156.

Fu, Q., Liou, K. N., Cribb, M. C., Charlock, T. P., & Grossman, A. (1997, December). Multiple Scattering Parameterization in Thermal Infrared Radiative Transfer. *J. Atmos. Sci.*, *54*(24), 2799–2812.

Garand, L., Turner, D. S., Larocque, M., Bates, J., Boukabara, S., Brunel, P., . . . Woolf, H. (2001, October). Radiance and Jacobian intercomparison of radiative transfer models applied to HIRS and AMSU channels. *J. Geophys. Res.*, *106*(D20), 24017–24031.

Goody, R., West, R., Chen, L., & Crisp, D. (1989, December). The correlated-k method for radiation calculations in nonhomogeneous atmospheres. *J. Quant. Spectrosc. Radiat. Transfer*, *42*(6), 539–550.

Gregory, J. M. (2004). A new method for diagnosing radiative forcing and climate sensitivity. *Geophys. Res. Lett.*, *31*(3), 147.

Hogan, R. J. (2010, June). The Full-Spectrum Correlated-k Method for Longwave Atmospheric Radiative Transfer Using an Effective Planck Function. *J. Atmos. Sci.*, *67*(6), 2086–2100.

Hogan, R. J., & Bozzo, A. (2018, August). A Flexible and Efficient Radiation Scheme for the ECMWF Model. *J. Adv. Model. Earth Syst.*, *10*(8), 1990–2008.

Hogan, R. J., Schäfer, S. A. K., Klinger, C., Chiu, J. C., & Mayer, B. (2016, July).

Representing 3-D cloud radiation effects in two-stream schemes: 2. Matrix formulation and broadband evaluation. *J. Geophys. Res.*, *121*(14), 8583–8599.

Iacono, M. J., Mlawer, E. J., Clough, S. A., & Morcrette, J.-J. (2000, June). Impact of an improved longwave radiation model, RRTM, on the energy budget and thermodynamic properties of the NCAR community climate model, CCM3. *J. Geophys. Res.*, *105*(D11), 14873–14890.

Joseph, J. H., Wiscombe, W. J., & Weinman, J. A. (1976, December). The Delta-Eddington Approximation for Radiative Flux Transfer. *J. Atmos. Sci.*, *33*(12), 2452–2459.

Kuo, C.-P., Yang, P., Huang, X., Feldman, D., Flanner, M., Kuo, C., & Mlawer, E. J. (2017, December). Impact of Multiple Scattering on Longwave Radiative Transfer Involving Clouds. *J. Adv. Model. Earth Syst.*, *9*(8), 3082–3098.

Lacis, A. A., & Oinas, V. (1991). A description of the correlated k-distribution method for modeling non-grey gaseous absorption, thermal emission, and multiple scattering in vertically inhomogeneous atmospheres. *J. Geophys. Res.*, *96*(D5), 9027–9063.

Lean, J. L., & DeLand, M. T. (2012, April). How Does the Sun's Spectrum Vary? *J. Climate*, *25*(7), 2555–2560.

Meador, W. E., & Weaver, W. R. (1980). Two-Stream Approximations to Radiative Transfer in Planetary Atmospheres: A Unified Description of Existing Methods and a New Improvement. *J. Atmos. Sci.*, *37*(3), 630–643.

Mlawer, E. J., Brown, P. D., Clough, S. A., Harrison, L. C., Michalsky, J. J., Kiedron, P. W., & Shippert, T. (2000, September). Comparison of spectral direct and diffuse solar irradiance measurements and calculations for cloud-free conditions. *Geophys. Res. Lett.*, *27*(17), 2653–2656.

Mlawer, E. J., Payne, V. H., Moncet, J. L., Delamere, J. S., Alvarado, M. J., & Tobin, D. C. (2012, April). Development and recent evaluation of the MTCKD model of continuum absorption. *Phil. Trans. Royal Soc. A*, *370*(1968), 2520–2556.

Mlawer, E. J., Taubman, S. J., Brown, P. D., Iacono, M. J., & Clough, S. A. (1997, July). Radiative transfer for inhomogeneous atmospheres: RRTM, a validated correlated-k model for the longwave. *J. Geophys. Res.*, *102*(D14), 16663–16682.

Oreopoulos, L., Mlawer, E., Delamere, J., Shippert, T., Cole, J., Fomin, B., . . .

Rossow, W. B. (2012, March). The Continual Intercomparison of Radiation Codes: Results from Phase I. *J. Geophys. Res.*, *117*, D06118.

Pincus, R., Barker, H. W., & Morcrette, J.-J. (2003). A fast, flexible, approximate technique for computing radiative transfer in inhomogeneous cloud fields. *J. Geophys. Res.*, *108*(D13), 4376–n/a.

Pincus, R., Forster, P. M., & Stevens, B. (2016). The Radiative Forcing Model Intercomparison Project (RFMIP): experimental protocol for CMIP6. *Geosci. Model Dev.*, *9*, 3447–3460.

Pincus, R., Mlawer, E. J., Oreopoulos, L., Ackerman, A. S., Baek, S., Brath, M., . . . Schwarzkopf, D. M. (2015, July). Radiative flux and forcing parameterization error in aerosol-free clear skies. *Geophys. Res. Lett.*, *42*(13), 5485–5492.

Pincus, R., & Stevens, B. (2009). Monte Carlo Spectral Integration: a consistent approximation for radiative transfer in large eddy simulations. *J. Adv. Model. Earth Syst.*, *1*(2), n/a–n/a.

Pincus, R., & Stevens, B. (2013, May). Paths to accuracy for radiation parameterizations in atmospheric models. *J. Adv. Model. Earth Syst.*, *5*(2), 225–233.

Potter, J. F. (1970, September). The Delta Function Approximation in Radiative Transfer Theory. *J. Atmos. Sci.*, *27*(6), 943–949.

Randles, C. A., da Silva, A. M., Buchard, V., Colarco, P. R., Darmenov, A., Govindaraju, R., . . . Flynn, C. J. (2017, September). The MERRA-2 Aerosol Reanalysis, 1980 Onward. Part I: System Description and Data Assimilation Evaluation. *J. Climate*, *30*(17), 6823–6850.

Rothman, L. S., Gordon, I. E., Babikov, Y., Barbe, A., Chris Benner, D., Bernath, P. F., . . . Wagner, G. (2013, November). The HITRAN2012 molecular spectroscopic database. *J. Quant. Spectrosc. Radiat. Transfer*, *130*(0), 4–50.

Rothman, L. S., Gordon, I. E., Barbe, A., Benner, D. C., Bernath, P. F., Birk, M., . . . Vander Auwera, J. (2009, June). The HITRAN 2008 molecular spectroscopic database. *J. Quant. Spectrosc. Radiat. Transfer*, *110*(9–10), 533–572.

Schäfer, S. A. K., Hogan, R. J., Klinger, C., Chiu, J. C., & Mayer, B. (2016, July). Representing 3-D cloud radiation effects in two-stream schemes: 1. Longwave considerations and effective cloud edge length. *J. Geophys. Res.*, *121*(14), 8567–8582.

Seifert, A., Heus, T., Pincus, R., & Stevens, B. (2015, December). Large-eddy simulation of the transient and near-equilibrium behavior of precipitating shallow

convection. *J. Adv. Model. Earth Syst.*, *7*(4), 1918–1937.

Sekiguchi, M., & Nakajima, T. (2008, November). A k-distribution-based radiation code and its computational optimization for an atmospheric general circulation model. *J. Quant. Spectrosc. Radiat. Transfer*, *109*(17-18), 2779–2793.

Shonk, J. K. P., & Hogan, R. J. (2008, June). Tripleclouds: An Efficient Method for Representing Horizontal Cloud Inhomogeneity in 1D Radiation Schemes by Using Three Regions at Each Height. *J. Climate*, *21*(11), 2352–2370.

Tan, Z., Lachmy, O., & Shaw, T. A. (2019, March). The sensitivity of the jet stream response to climate change to radiative assumptions. *J. Adv. Model. Earth Syst.*, *0*(ja), 2018MS001492.

Turner, D. D., Tobin, D. C., Clough, S. A., Brown, P. D., Ellingson, R. G., Mlawer, E. J., . . . Shephard, M. W. (2004, November). The QME AERI LBLRTM: A Closure Experiment for Downwelling High Spectral Resolution Infrared Radiance. *J. Atmos. Sci.*, *61*(22), 2657–2675.

Vallis, G. K., Colyer, G., Geen, R., Gerber, E., Jucker, M., Maher, P., . . . Thomson, S. I. (2018). Isca, v1.0: a framework for the global modelling of the atmospheres of Earth and other planets at varying levels of complexity. *Geosci. Model Dev.*, *11*(3), 843–859.

Wiscombe, W. J., & Evans, J. W. (1977, August). Exponential-sum fitting of radiative transmission functions. *J. Comp. Phys.*, *24*(4), 416–444.

Yang, J., Leconte, J., Wolf, E. T., Goldblatt, C., Feldl, N., Merlis, T., . . . Abbot, D. S. (2016). Differences in Water Vapor Radiative Transfer among 1D Models Can Significantly Affect the Inner Edge of the Habitable Zone. *Ap. J.*, *826*(2), 222.

Zdunkowski, W. G., Welch, R. M., & Korb, G. J. (1980, September). An investigation of the structure of typical two-stream methods for the calculation of solar fluxes and heating rates in clouds. *Beiträge zur Physik Atmosphäre*, *53*, 147–166.
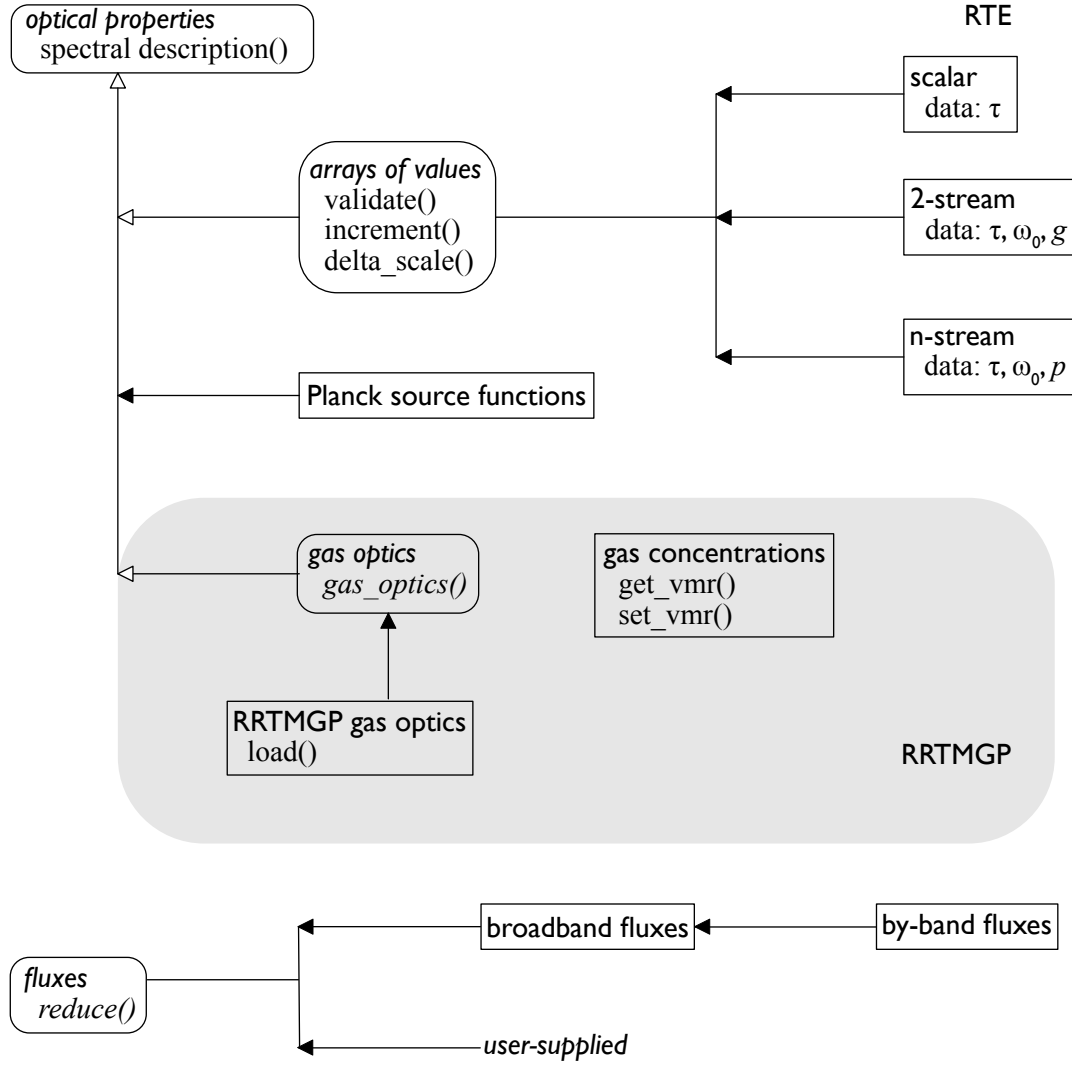
Figure 1. Class organization for RTE+RRTMGP. Class names are in sans serif fonts, data and procedures in serif. Arrows indicate inheritance: classes inherit the data and procedures and/or interfaces provided by their parents. Ovals, open arrowheads, and italicized class names represent abstract classes providing functionality and/or specifying procedures to be provided by descendent classes. Calculations require concrete classes (un-italicized names, rectangles). Solvers are implemented as procedures using these classes as inputs or to compute outputs. The figure illustrates only the most important functionality within each class; most implement more procedures than are shown.
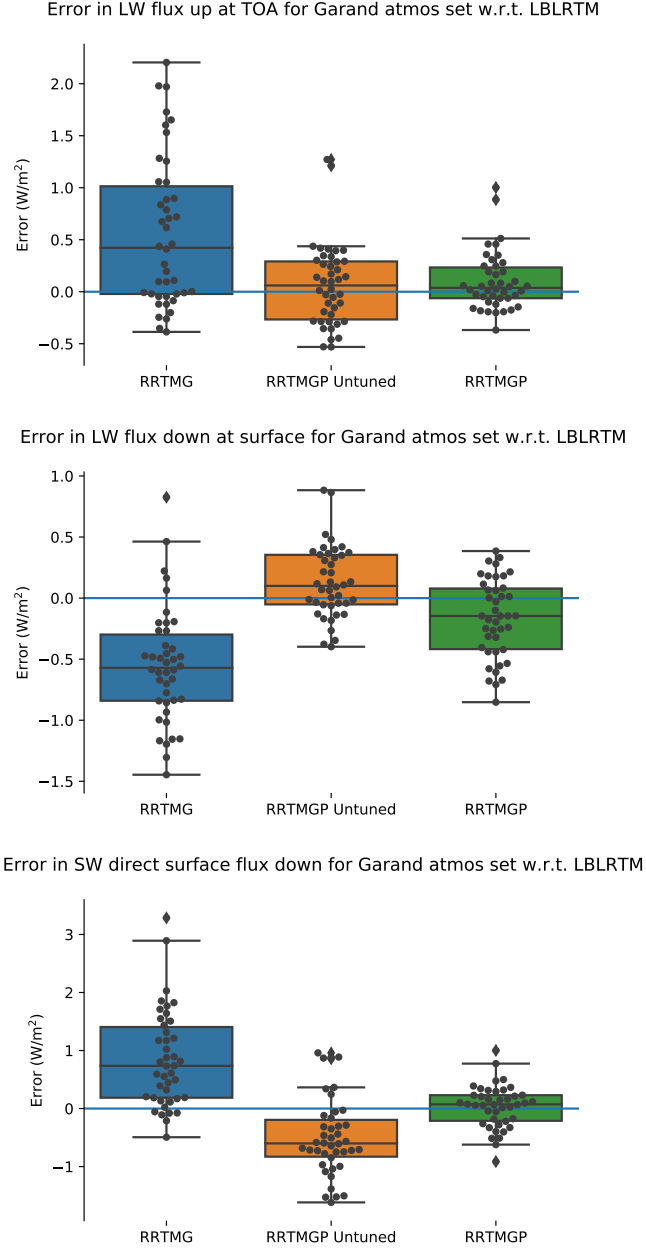
Figure 2. Accuracy of RRTMGP's new k-distribution, assessed as the difference between fluxes computed with RTE+RRTMGP and those from the reference calculations across the set of training atmospheres. Longwave calculations compare high spectral resolution line-by-line and parameterized calculations using identical transport algorithms while the shortwave comparison focused only on the direct solar beam at the surface and so requires no multiple-scattering calculations.
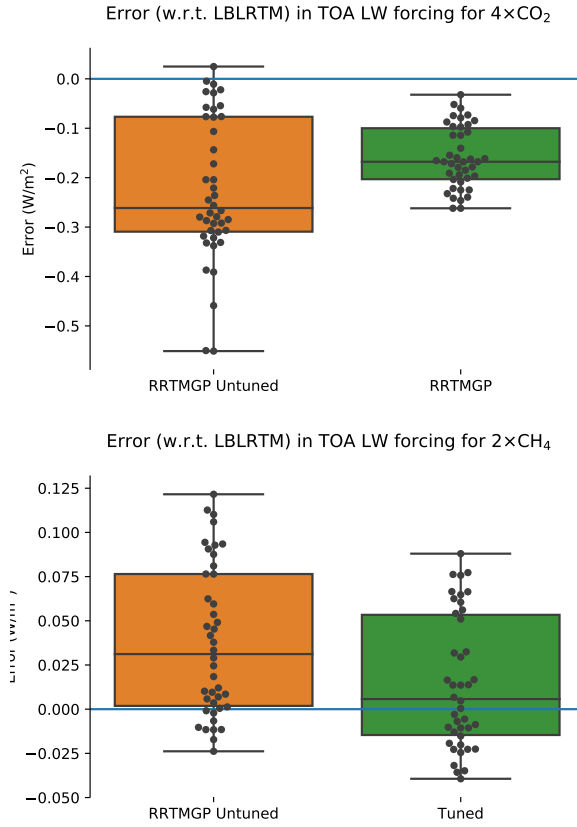
Figure 3. Accuracy of RRTMGP's new k-distribution for forcing calculations. Shown here are the two primary forcings considered during tuning: impacts on top-of-atmosphere longwave fluxes from concentrations of carbon dioxide quadrupled from pre-industrial concentrations, and doubled methane concentrations. As with fluxes, tuning reduces the largest errors and modestly improves the median error across the training dataset.
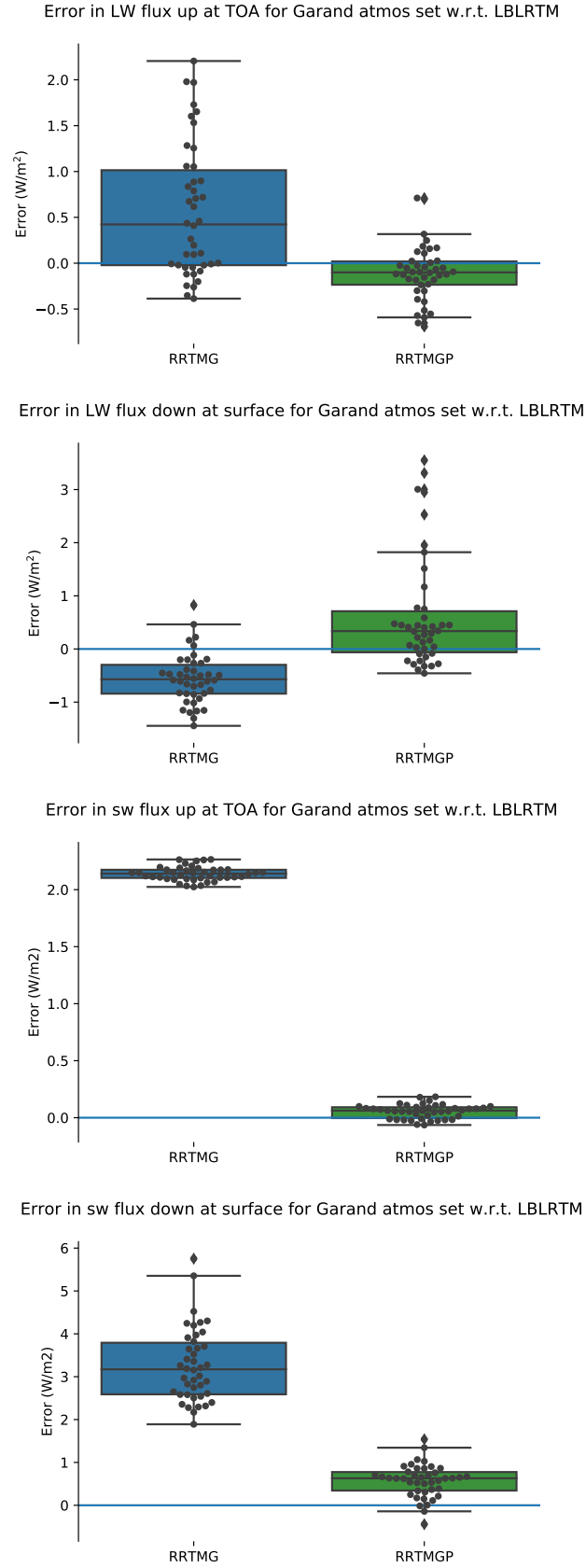
Figure 4. Accuracy of RTE+RRTMGP in producing fluxes at the surface and top-of-atmosphere as judged against line-by-line calculations on the set of training atmospheres. RTE

uses a single angle calculation (c.f. the three-angle calculation in Fig. 2) for the longwave calcula-
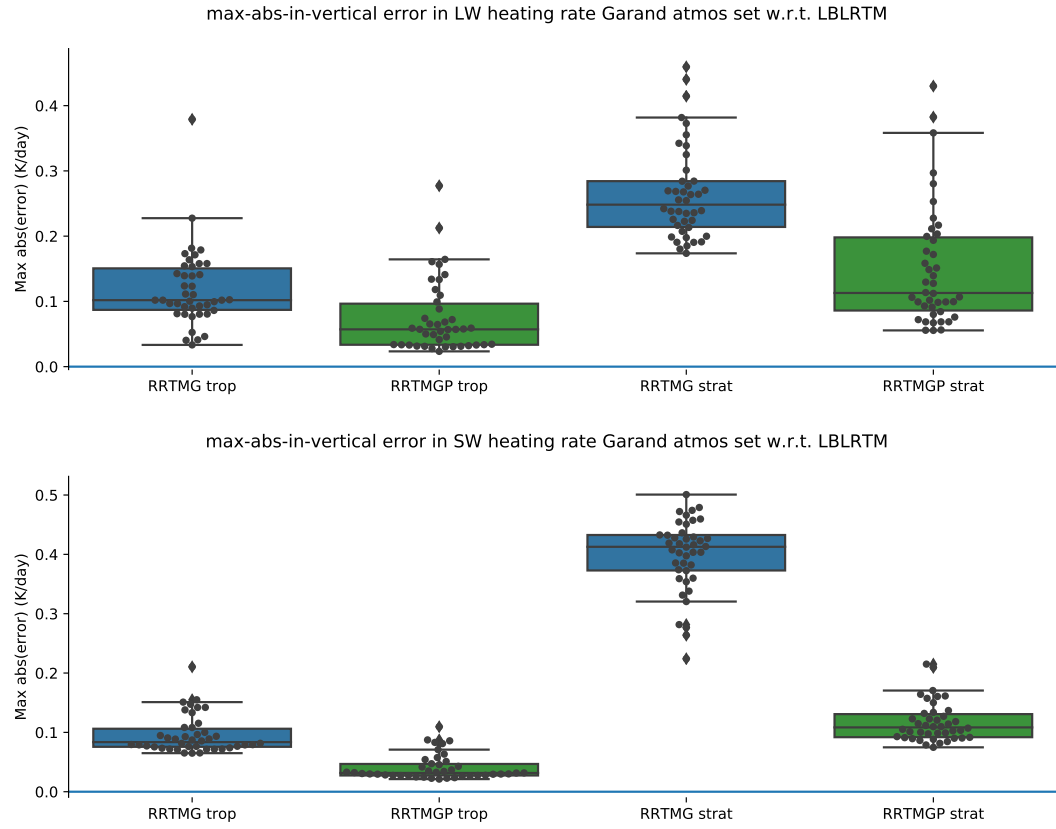
Figure 5. Accuracy of RTE+RRTMGP in producing heating rates.